Collective ionic dynamics in a molten binary alloy

R. Férnandez-Perea, M. Alvarez, and F. J. Bermejo

Instituto de Estructura de la Materia, Consejo Superior de Investigaciones Científicas, Serrano 119-123, E-28006 Madrid, Spain

P. Verkerk

Interfacultair Reactor Instituut, TU-Delft, 2629 JB Delft, The Netherlands

B. Roessli

Laboratory for Neutron Scattering, PSI, ETH Zurich, Switzerland

E. Enciso

Departamento de Química-Física I, Universidad Complutense, E-28040 Madrid, Spain

A recent experiment [Phys. Rev. Lett. **80**, 2141 (1998)] showed heavily damped excitations in molten Li_4Pb, within kinematic scales well beyond those of hydrodynamic sound. These findings pointed to the presence of short-lived out-of-phase atomic motions as the underlying microscopic phenomenon. A series of computer molecular dynamics studies are performed to investigate the details of the atomic motions. From an analysis of the simulated structure factors for molten Li_4Pb, as well as by a comparison with those of liquid Li under different thermodynamic conditions, it is found that the high-frequency excitation found in the alloy shows characteristics remarkably different from those of pure Li. The relative phases of the atoms partaking in such motions, as well as the remarkably short excitation lifetimes, portray it as a fairly localized mode, with a frequency dependent polarization. [S1063-651X(98)07210-9]

I. INTRODUCTION

Molten metallic alloys, within which atoms of type *A* are very strongly attracted by others of type *B*, have been investigated for many decades as a consequence of their rather particular thermodynamic and structural properties [1]. From the point of view of the change in electronic structure upon melting, such liquids are in between those fully ionized insulating salts, which remain ionic after melting of the parent crystal, and those covalent semiconducting solids such as Ge or Ga where the covalent character gives way, upon melting, to a liquid with a more marked metallic character. Examples of this are Cs-Au or Li-Pb and other alloys of alkalis with Pb, In, or Tl [2]. The available evidence portrays the structure of such liquids as leading to compound formation near the *AB* (equimolar) or A_4B octet compositions, depending upon the metallic elements. For the $^7Li_4Pb$ sample under consideration, the octet composition leads to a maximum in the electrical resistivity [3] concomitant with a strong decrease of long-wavelength concentration fluctuations [4]. The liquid retains its metallic character, although measurements of some electrical transport properties indicate that it is not far from a metal-insulator transition [1].

A number of detailed neutron, x-ray, and theoretical investigations have been carried to unveil the microscopic structure of the liquid [5]. These show the signatures of strong chemical short-range order in the derived static pair correlation functions which translates into a first intense peak at 2.9 Å, indicative of strong Li-Pb correlations, a distance which becomes about 5% shorter than that of equilibrium Li-Li correlations. The question of whether such atomic arrangements are stable or not has, to the authors' knowledge, not been answered in full. In fact, the experimental liquid structure factor can be reproduced by means of calculations without explicit inclusion of overlap interactions between Li and Pb [5]. Indeed, as shown by Nixon and Silbert [5], a basic ordering mechanism can arise, in a mixture of spheres of disparate diameters, from the nonadditivity effects (breakdown of Lorentz-Berthelot rules). The most widely accepted view thus seems to regard bonding in this liquid as resulting from a valence band, where the outer Pb *p*-electron states join with electrons from the Li 2*s* band, a process mediated by charge-transfer, leading to a minimum (not a gap) in the electronic density of states at the Fermi level. On the other hand, estimates from analysis of quasielastic neutron scattering data [6] put an upper bound for the lifetime of the Li_4Pb ''molecules'' of about 1 ps.

The dynamics of molten $^7Li_4Pb$ was first investigated by cold neutron scattering [6]. The total neutron scattering cross section for a molten binary alloy such as Li_4Pb composed of particles with percentage concentrations c and $(1-c)$ is given by [7]

$$\frac{d^2\sigma}{d\Omega dE} = N\frac{k'}{k}[1+n(\omega)]\omega\beta\left\{[c\bar{b}_{Li}+(1-c)\bar{b}_{Pb}]^2R(Q,\omega)\right.$$

$$\left.+c(1-c)(\bar{b}_{Li}\bar{b}_{Pb})^2+\frac{c\sigma_{Li}^{inc}}{4\pi}R_s(Q,\omega)\right\}. \quad (1)$$

Here N stands for the total number of particles, the flux factor k'/k represents the density of final neutron states over the incident neutron flux, $1+n(\omega)$ is the Bose factor, and the response functions $R(Q,\omega)$ are defined in a way that approach as the $S(Q,\omega)$ dynamic structure factor in the classi-

cal limit; that is, $S(Q,\omega) = 1 + n(\omega)\omega\beta$, where $\beta = (k_B T)^{-1}$. The quantities $\bar{b}_i$ stand for coherent scattering length for the ith atomic species, whereas σ_{Li}^{inc} stands for the total incoherent cross section for ^{7}Li (that for Pb is negligible). The coherent response $R(Q,\omega)$ is in turn decomposed into partials,

$$R(Q,\omega) = c(\bar{b}_{Li})^2 R_{LiLi}(Q,\omega)$$
$$+ 2c(1-c)^{1/2}\bar{b}_{Li}\bar{b}_{Pb}R_{LiPb}(Q,\omega)$$
$$+ (1-c)(\bar{b}_{Pb})^2 R_{PbPb}(Q,\omega), \qquad (2)$$

whereas, as stated above, only Li will contribute to the incoherent response which is expected to be concentrated at frequencies about zero (quasielastic scattering). Other decompositions of the total response have been used and, in fact, that given in terms of correlation functions for the density $R_{\rho\rho}(Q,\omega)$, concentration $R_{cc}(Q,\omega)$ and their respective cross terms has proven useful for the analysis of low-Q (quasielastic scattering) data [6]. The equivalence between both formulations is given by [7]

$$R(Q,\omega) = [c\bar{b}_{Li} + (1-c)\bar{b}_{Pb}]^2 R_{\rho\rho}(Q,\omega)$$
$$+ 2(\bar{b}_{Li} - \bar{b}_{Pb})[c\bar{b}_{Li} + (1-c)\bar{b}_{Pb}]R_{\rho\rho}(Q,\omega)$$
$$+ (\bar{b}_{Li} - \bar{b}_{Pb})^2 R_{cc}(Q,\omega). \qquad (3)$$

In the case under scrutiny, the equation given above is substantially simplified, since the average scattering length $\langle b \rangle = c\bar{b}_{Li} + (1-c)\bar{b}_{Pb} = 0$ ($c\bar{b}_{Li} = -0.229$ fm, $\bar{b}_{Pb} = 0.94$ fm, and $c = 0.8$); thus only $R_{cc}(Q,\omega)$ contributes to the spectrum, which in turn contains

$$R_{cc}(Q,\omega) = c(1-c)[(1-c)R_{LiLi}(Q,\omega)$$
$$- 2c(1-c)^{1/2}R_{LiPb}(Q,\omega) + cR_{PbPb}(Q,\omega),$$
$$\qquad (4)$$

which are terms governing the dynamics of the two components, plus a cross-term which at low frequencies and wave vectors represent a microscopic interdiffusion contribution.

The experimental data for low energies [6] show that incoherent scattering from ^{7}Li [i.e., the $R_s(Q,\omega)$ term in Eq. (1)] dominates the low-frequency spectrum up to wave vectors ≈ 0.7 Å^{-1} that is, midway to the coherent peak in $R_{cc}(Q,\omega)$ which appears at ≈ 1.5 Å^{-1}. Data analysis of the incoherent quasielastic region (below 0.5 Å^{-1}) performed on hydrodynamic (Fick's law) grounds yielded ^{7}Li self-diffusion coefficients ranging between 17.5×10^{-5} cm^2/s at 1023 K to 27.4×10^{-5} cm^2/s at 1173 K [6], which are about 1.5 times lower than those of pure Li metal extrapolated at such temperatures, and the apparent activation energy also turns out to be far higher than that of molten Li. The macroscopic interdiffusion coefficient D^+ was evaluated by recourse to a phenomenological extension of the hydrodynamic Darken's relation (Lorentzian response) to finite Q [6]. This allowed the determination of the Pb self-diffusion coefficient (too weak to be directly measurable) which was

found to be 6–8 times smaller than that of Li, but comparable to the interdiffusion coefficient.

The dynamics at larger frequencies and wave vectors was first investigated by computer molecular dynamics simulations [8]. The main interest was focused on the study of a high-frequency peak appearing in $R_{cc}(Q,\omega)$, centered at frequencies which, if interpreted in terms of the phase velocity of a propagating acoustic wave, would lead to a velocity $\omega_Q/Q = 7500$ m/s, whereas the hydrodynamic sound for the mixture travels at about 2000 m/s, and indeed it is also much faster than the propagation velocity in liquid Li [9] which never exceeds 4500 m/s.

The existence of an excitation with frequencies well above that of hydrodynamic sound in the liquid referred to above was inferred from preliminary neutron work [10], and later confirmed in a more detailed hot-neutron spectroscopy study [11]. Both studies unveiled a heavily damped inelastic wing, which, below $Q_{LiLi}/2 \approx 1.5$ Å^{-1}, that is halfway to the maximum of the $S_{LiLi}(Q)$ structure factor, seems to follow the "dispersion curve" of pure Li. To picture such an excitation as high-frequency sound [8] is, however, in contrast to the wave vector dependence of its intensity, which behaves in a way somewhat reminiscent of that for an "optic" mode in a liquid, in much the same way as found for some molten salts [12].

Our aim here is then to explore the high-frequency dynamics in molten Li$_4$Pb in those aspects which are difficult to access from experiment. The main emphasis will be placed on a detailed characterization of the "geometry" of atomic motions, as well as on a comparison between some of the dynamical features exhibited by molten metallic Li and those found for the Li-Li dynamic correlations in the alloy. To achieve this, molecular dynamics simulations are carried using the same potential as that used in Ref. [8], and the spectra are analyzed in ways fully equivalent to those employed to treat the experimental data. On the other hand, particular attention is paid to the analysis of the inelastic structure factors which, once inverted into real space, will provide detailed information on the relative phases of the atomic oscillations.

II. COMPUTER SIMULATION AND DATA ANALYSIS DETAILS

As known from previous quasielastic experiments [6], as well as from measurements on pure liquid Pb [13], the partial $R_{PbPb}(Q,\omega)$ is bound to frequencies below ≈ 10 meV. Experimentally [11] it contributes to the resolution-broadened quasielastic peak. The same applies to the quasielastic part of $R_{LiLi}(Q,\omega)$, $R_{LiPb}(Q,\omega)$, and $R_s^{inc}(Q,\omega)$, as commented upon above. The $R_{LiPb}(Q,\omega)$ term in the Eq. (1) cross-correlation has a small negative weight, and its range [8] will also be confined to frequencies below ≈ 13 meV. As a consequence, the high-frequency part of $R_{LiLi}(Q,\omega)$ becomes very close to $R_{cc}(Q,\omega)$, as given by Eq. (4).

The model used in Ref. [11] to fit the experimental intensities included a term accounting from all quasielastic scattering processes, which is approximated by a hydrodynamic prescription specified by an amplitude Z_q and linewidth γ_q as

$$R_{q-el}(Q,\omega) = Z_q \frac{\gamma_q}{\omega^2 + \gamma_q^2}, \tag{5}$$

where, as stated above, all contributions below about 10–12 meV were lumped together. In addition, the collective dynamics was described in terms of a damped harmonic oscillator [14]

$$R(Q,\omega) = \frac{I_Q}{2\pi} \frac{4\omega_Q \Gamma_Q}{(\omega^2 - \Omega_Q^2)^2 + 4\omega^2 \Gamma_Q^2} \tag{6}$$

defined in terms of an excitation strength I_Q, frequency $\Omega_Q = \sqrt{\omega_Q^2 + \Gamma_Q^2}$ and a linewidth which is the inverse of the excitation lifetime, $\Gamma_Q = \tau_Q^{-1}$. The functional form chosen above for $R(Q,\omega)$ enables a formal identification of Ω_Q with that corresponding to maxima of the longitudinal current correlation function $J_l(Q,\omega) = (\omega^2/Q^2)R(Q,\omega)$, which is the quantity plotted in the ''dispersion curves'' of previous simulation works. Both quantities can be equated, provided that the whole spectrum is describable by only one oscillator. On the other hand, it provides a physically appealing form for a modal frequency in a dissipative environment (i.e., the ''bare'' frequency ω_Q is renormalized by the anharmonic interactions [14]).

Computer simulations

The purpose of the computer simulations here is to provide a more detailed characterization of the excitations by means of analysis of quantities not easily amenable to experiment, and also to help clarify the relationship between the dynamics of molten Li_4Pb and that of its pure molten constituents, especially that of liquid Li. The comparison is relevant since kinetic theory portrays the ''fast sound mode'' as sustained by the Li atoms only [15], and therefore finding a propagation velocity such as that of ''fast sound'' close to twice the value of sound velocity in liquid Li needs to be explained. With such an aim, several simulations were carried out for molten Li_4Pb under conditions resembling those employed in the experiments, as well as for liquid Li at a thermodynamic state close to that explored by experiment [9] and also on a sample on liquid Li having the same density and temperature of Li_4Pb.

In all cases the effective potential used for the simulations corresponds to the model of Copestake *et al.* [5], with interaction parameters set to values given in Ref. [8]. Several different simulations were carried for three systems: Li_4Pb at a density and temperature mimicking experiment ($\rho = 0.0443$ Å^{-3}, $T = 1050$ K), a sample representing liquid Li just above melting ($\rho = 0.0447$ Å^{-3}, $T = 473$ K), and a final one which would correspond to liquid Li, under density and temperature conditions equivalent to Li within the alloy. Simulation runs were carried using different box sizes. The basic box was a cube of 21.2 Å per side, and different calculations were performed employing simulation cells formed by juxtaposition of four, eight, or 16 of such units. In the latter case the simulation cell is thus constituted by a parallelepiped of $338.6 \times 21.2 \times 21.2$ Å^3 containing 6720 particles. This enabled us to reach wave vectors as low as 0.019 Å^{-1}, corresponding to the largest distance within

such cells. Finite-size effects were investigated by means of simulations carried with boxes of different sizes (four, eight, and 16 blocks). Simulation runs were carried over 0.25 ns employing a time step of 5 fs.

The calculation of the relevant quantities followed well established procedures. The ensuing discussions will be centered about $R(Q,\omega)$ or $S(Q,\omega)$ without further distinction, since the simulation is carried on fully classical grounds ($\hbar \to 0$). The decomposition of the atomic dynamics into instantaneous normal modes was carried out using procedures analogous to those employed previously [16].

In what follows we will follow the advice of March and Tosi [17], and stick to the decomposition of the total response in terms of partial correlations, since it presents some advantages for the analysis of large-Q data. The analysis of the simulation data has been carried following different routes. On the one hand, a model-free analysis was carried on the basis of peak frequencies of $J_l(Q,\omega) = \omega^2 R(Q,\omega)/Q^2$ longitudinal current correlations for the total spectra. This allows a connection with experiment, since such frequencies are equivalent to those Ω_Q derived from fits of damped harmonic oscillator response functions to the high-frequency wings. On the other hand, the analysis of the spectral line shapes is also carried in the same way employed to analyze the experimental data, that is modeling the quasi-elastic and inelastic intensities by recourse to formulas such as Eqs. (5) and (6).

A physically more appealing approach takes recourse to a calculation of the first two reduced spectral frequency moments of the total as well as partial spectra. This enables a model-free assessment of the small- and large-Q behaviors of quantities which now have a clear physical meaning as sum rules. Furthermore, the spectral line shape can also be approximated in terms of the second and fourth reduced moments of the $R(Q,\omega)$ response functions, plus an additional parameter (the relaxation time). Limiting ourselves to the correlations of interest which involve Pb-Pb and Li-Li pairs (the cross-correlation is bounded to small frequencies), the moments of the $R_{ii}(Q,\omega)$, $i = $Li or Pb, partial response functions are defined in terms of the quantities $\langle \omega^n \rangle$ as,

$$\omega_0^2(i) = \frac{\langle \omega_{ii}^2 \rangle}{S_{ii}(Q)} = \frac{1}{S_{ii}(Q)} \int d\omega\, \omega^2 R_{ii}(Q,\omega),$$

$$\tag{7}$$

$$\omega_l^2(i) = \frac{\langle \omega_{ii}^4 \rangle}{\langle \omega_{ii}^2 \rangle} = \frac{\int d\omega\, \omega^4 R_{ii}(Q,\omega)}{S_{ii}(Q)\omega_0^2(i)}.$$

Both quantities could, in principle, be interpreted as those characteristic of a fluid where, within some kinematic conditions, the dynamics of both atomic species could be regarded as decoupled [18]. With such a proviso these quantities would have well defined hydrodynamic limits given in terms of the isothermal sound velocity $v_T(i)$, wave vector dependent bulk $B(i)$, and longitudinal moduli $C_{11}(i)$ and mass density $M_i\rho_i$ for the i component of the alloy:

$$\lim_{Q\to 0} \omega_0^2(i) = Q^2 v_T^2(i), \tag{8}$$

$$Q^2 C_{11}(Q) = M_i \rho_i \omega_l^2(i), \qquad (9)$$

$$\lim_{Q \to 0} C_{11}(Q) = B(i) + \tfrac{4}{3} G(i), \qquad (10)$$

where $G(i)$ stands for the rigidity modulus. An absolute, high-frequency limit is also given by $\sqrt{(B(i) + \tfrac{4}{3} G(i))/M_i \rho_i}$. At large momentum transfers both reduced frequency moments are expected to approach their ideal-gas limits given by

$$\lim_{Q \to \infty} \omega_0(i) = \hbar Q \left(\frac{k_B T}{M_i} \right)^{1/2}, \qquad (11)$$

$$\lim_{Q \to \infty} \omega_l(i) = \hbar Q \left(\frac{3 k_B T}{M_i} \right)^{1/2}, \qquad (12)$$

in terms of momentum transfer and thermal velocities.

The spectral shapes can be approximated by modeling the $R_{ii}(Q,\omega)$ response functions in terms of the three-pole approximation [7]

$$R_{ii}(Q,\omega) = \frac{1}{\pi} \frac{S_{ii}(Q) \omega_0^2(i) (\omega_l^2(i) - \omega_0^2(i)) \tau(i)}{[\omega \tau(i)(\omega^2 - \omega_l^2(i))]^2 + (\omega^2 - \omega_0^2(i))^2}, \qquad (13)$$

which is defined in terms of the two frequency moments: a Q-dependent intensity which should follow the $S_{ii}(Q)$ static partial structure factor, and a relaxation time $\tau(i)$. In the course of the analysis it was found that an accurate reproduction of the line shapes required leaving the relaxation time as an adjustable parameter rather than making recourse to the viscoelastic approximation which links the relaxation time with the two frequency moments.

Having access to spectra which are free of kinematic and instrument-response limitations enables us to compute some quantities which contain information regarding the spatial extent as well as on the relative phases of the atomic motions. To see this, consider the structure factors $S_{ij}(Q,\omega = \text{const})$ for the different partial correlations and for selected values of the energy transfers. At the high frequencies of interest the liquid can be expected to behave as an elastic body, and, consequently, the constant-energy structure factors can be interpreted in terms of inelastic structure factors which can provide some details about the *geometry* of the atomic vibrations, that is about the relative phases of the atomic vibrational displacements. In fact, a transform of an inelastic structure factor can be defined [19] as

$$D(r,\omega^\lambda) = \frac{2}{\pi} \int_0^\infty dQ \, Q \sum_{l,m} F_{l,m}^\lambda(Q) \sin(Qr), \qquad (14)$$

where the sum runs over l,m atom pairs participating in the λth normal mode, and $F_{l,m}^\lambda(Q)$ stands for an inelastic structure factor. The meaning of $D(r,\omega = 0^\lambda)$ is obvious; it corresponds to the static spatial correlation functions of atoms obtained by Fourier inversion of $(S_{ij}(Q) - 1)$. The peak positions of such a function will then correspond to average distances between atoms in the static structure. At a given frequency, $F_{l,m}^\lambda(Q)$, is given by

$$\frac{F_{l,m}^\lambda(Q)}{Q^2} = \frac{1}{\sqrt{M_l M_m}} \left[\frac{1}{3} (\boldsymbol{\gamma}_l^\lambda \cdot \boldsymbol{\gamma}_m^{\lambda *}) j_0(Q d_{l,m}) \right.$$
$$\left. + \left(\frac{1}{3} (\boldsymbol{\gamma}_l^\lambda \cdot \boldsymbol{\gamma}_m^{\lambda *}) - \frac{1}{d_{l,m}^2} (\mathbf{d}_{l,m} \cdot \boldsymbol{\gamma}_m^{\lambda *}) \right) j_2(Q d_{l,m}) \right] \qquad (15)$$

As can readily be seen, such a function will show oscillations arising from combinations of the $j_{0,2}$ spherical Bessel functions the products involving $\boldsymbol{\gamma}_l^\lambda$ atomic vector displacements and the $\mathbf{d}_{l,m}$ internuclear distance vectors. At low frequencies, it is expected that such an oscillatory structure follows $Q^2 S(Q)$, a consequence derived from motions (sound waves) that leave the characteristic distances of the system unaffected. At higher frequencies, the structure in $F_{l,m}^\lambda(Q)$ will surely lose coherence with the static structure factor. That is, some of the peaks of the static structure will disappear, and a new structure may emerge at other positions. From the structure of Eq. (15), it may be seen that positive peaks in $D(r,\omega^\lambda)$, will result from motions of atom pairs where the displacements are in phase, whereas purely out-of-phase motions will result in negative peaks. As a consequence, inspection of the structure of such functions provides a convenient way to investigate the dominant character of excitations taking place at a given frequency.

III. RESULTS

In what follows we will first delve into the different ways in which one can characterize the wave vector dependence of the structure factors. The analysis of the line shapes of the total structure factor will allow us to establish some connections with the experiment. We will then follow with a more detailed analysis carried on the basis of the partial structure factors, which will help to unveil important details especially at low wave vectors. The intricate geometry of the atomic motions is explored by means of a calculation of the mode eigenvectors arising from a decomposition of the high-frequency dynamics into instantaneous normal modes. From there, inelastic form factors for single excitations are calculated, and the results, once transformed into real space, analyzed in terms of the relative phases of atomic oscillations taking place at a given frequency. Finally, a comparison of the dynamics of pure liquid Li and that of lithium within the alloy will be made for two thermodynamic states of the metallic sample.

A. Wave vector dependence of the spectra

The static structure factors which are evaluated as the zeroth frequency moments of the partial dynamic structure factors are shown in Fig. 1. Figure 2 displays the results regarding the analysis of the Li_4Pb partial spectra in terms of quantities defined by Eq. (7). The $\omega_0(i)$ curves are interpreted here as average excitation frequencies. Their relationship with those Ω_Q estimated from fits using Eq. (6) to the total spectra can be best gauged from Fig. 2(a), where both quantities are superposed. From there it is seen that both routes of analysis lead to quite similar results for Q values below 1.0 Å^{-1}. The discrepancy above such momentum
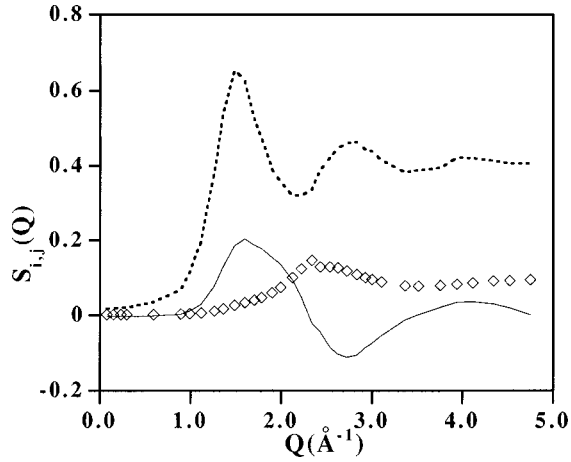
FIG. 1. Partial static structure factors for Li-Li (lozenges), Li-Pb (solid line), and Pb-Pb (dots) correlations calculated as $\langle \omega^0 \rangle$ moments of the $S_{ij}(Q,\omega)$ partial dynamic structure factors. Units are barns per atom.

transfers results from the increasing width of the spectrum as well as the reduction in its frequency, leading to the "roton" minimum at about 2.5 Å^{-1}. For comparison purposes, the experimental values reported in Ref. [11] are also plotted there, and the agreement with those Ω_Q estimated from the simulated spectra is shown to be good. The same applies to frequencies of peak maxima of $J_l(Q,\omega)$, the quantities plotted in previous simulation works [8].

In what follows the discussion will be focused onto the wave vector behavior of the reduced frequency moments. For a classical fluid sustaining heavily damped excitations, this approach seems more flexible than the damped oscillator because the behavior at large Q can be better understood within this framework.

As far as the physical meaning of $\omega_l(i)$, the quantity can be taken as a high-frequency limit for the sound velocity where the liquid would respond elastically. The existence of a propagating mode requires that [7]

$$3\omega_0^2 > \omega_l^2, \qquad (16)$$

a condition which is expected to hold at low wave vectors at least.

For both Pb-Pb and Li-Li correlations, if the interactions between Li and Pb were not too strong one would expect to find ω_0 and ω_l curves retaining in some respects some of the characteristics shown by the pure components. Within the hydrodynamic realm both curves should approach the linear sound dispersion regime for the mixture which is given by $\omega_s = v_T Q$, with v_T determined from the static structure factor via the isothermal compressibility equations, that is

$$v_T = (\chi_T M_{\text{av}} \rho)^{1/2}, \quad S(0) = \rho \chi_T k_B T, \qquad (17)$$

where $M_{\text{av}} = 0.8 M_{\text{Li}} + 0.2 M_{\text{Pb}}$ is the average atomic weight, and ρ stands for the average number density. Under such conditions the expectation would be to find curves for the spectral moments of both species behaving at low wave vectors, as given by Eq. (8), that is, as linear functions of the momentum transfer with velocities,
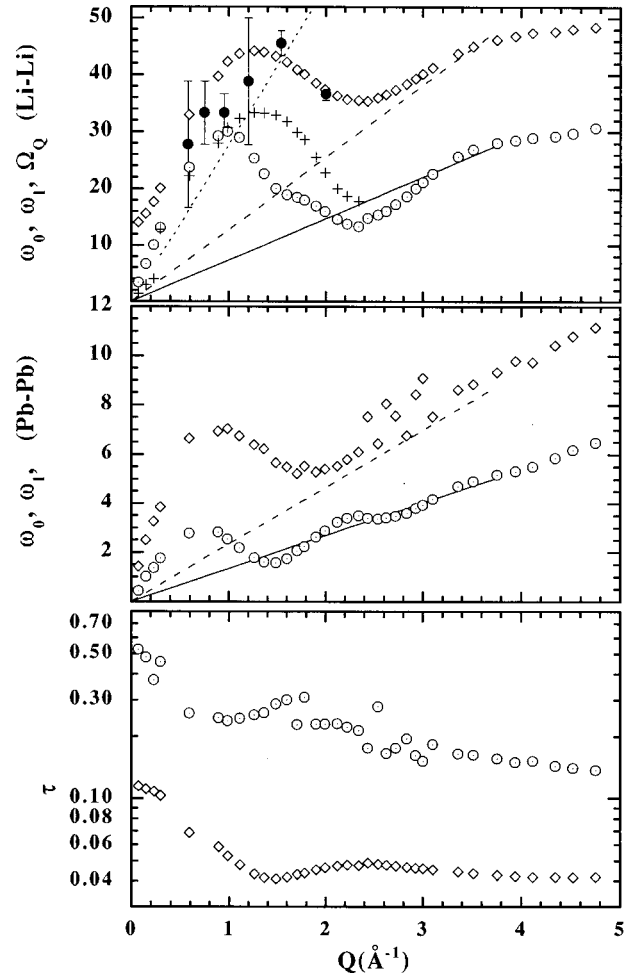

FIG. 2. The upper frame shows the reduced frequency moments (meV) ω_0 (circles), and ω_l (lozenges) of the $S_{\text{LiLi}}(Q,\omega)$ dynamic structure factor. The solid and long-dashed lines show the ideal-gas limits given by Eq. (12). The dotted line shows the hydrodynamic dispersion for liquid Li. Crosses show the Ω_Q renormalized excitation frequencies derived from fits of Eqs. (5) and (6) to the calculated structure factors. Filled circles with error bars stand for frequencies derived from fits to experimental spectra given in Ref. [11]. The middle frame shows the corresponding quantities for Pb-Pb correlations (equivalent symbols to those used for Li-Li correlations are employed). The lower frame shows the relaxation times τ for Pb-Pb (circles) and Li-Li (lozenges) correlations evaluated by recourse to the viscoelastic approximation (i.e., $\tau^{-1} = 2([\omega_l^2 - \omega_0^2]/\pi)^{1/2}$) from the moments of the simulated spectrum of the Li$_4$Pb alloy.

$$v_T(i) = v_T (M_{\text{av}}/M_i)^{1/2}, \qquad (18)$$

which are scalable from that for the mixture and modified by a mass factor [18]. On the other hand, it is also expected that the behavior at Q values well beyond Q_p approaches Eq. (11), ω_0 approaching such a limit at shorter wave numbers than ω_l.

Let's first consider the correlations arising from Pb-Pb atom pairs. The result shown in Fig. 2 indicates that the expectations referred to in the above paragraph are fulfilled. The Q dependence of both ω_0 and ω_l conforms to what could be expected for a "simple liquid" which shows a sound mode at low wave vectors. Such a behavior is also

extendable to the relaxation times, derived either by fitting the spectra or calculated by means of the viscoelastic approximation, which show a familiar shape, strongly decreasing from hydrodynamic values at low Q's and showing a minimum at Q_{Pb}, that is at wave vectors where the static structure factor shows its maximum. A remark seems in order here. It concerns the remarkably short time of the relaxation time as well as the derived values for the phase velocity. The latter goes from about 2200 m/s, and then decreases down to a well defined minimum at Q_{Pb}. The lifetime of the excitations can be estimated by the relaxation time, which decreases rather quickly upon entrance in the kinetic regime, and shows values within 0.5 and 2.5 Å^{-1} of the order of half a picosecond.

The amplitude of the low-frequency spectrum shows well defined oscillations in phase with the static structure factor. Moreover, both ω_0 and ω_l show an oscillatory structure with maxima not far from $Q_{Pb}/2$, local minima at Q_{Pb}, and a behavior at large wave vectors approaching the ideal-gas limits for a particle with a mass of 207.2 a.m.u. (M_{Pb}).

A rather distinctive behavior is followed by the Li-Li frequency moments. Although the curves for the frequency moments are reminiscent of those found for the Pb-Pb spectrum, (but shifted at higher frequencies), clear deviations from the interaction-free picture referred to above are seen in the shape of ω_l, and very especially its behavior at low wave vectors which displays a very clear limiting value at a finite frequency. Moreover, as will be illustrated below, the Q dependence of the amplitude of the inelastic part of the spectrum does not exhibit a maximum at Q_{Li}, and, finally, the relaxation time evaluated from the frequency moments approaches the hydrodynamic regime far too smoothly. If interpreted as the phase velocity of an excitation, $v_{ph} = \omega_0/Q$ would give an extremely high value (8400 m/s at 0.26 Å^{-1}) which decreases monotonously with Q (negative dispersion). That is, if such a frequency were assigned to a sound mode, then such a sonic excitation would show, within hydrodynamics (at $Q \to 0$), a velocity which is 3.8 times above the sound velocity of the alloy and about 1.9 times that of liquid Li, as we shall discuss below, and about 1.5 times higher than the longitudinal velocity in crystalline ${}^7\text{Li}$ [9].

Of particular relevance are the findings concerning the divergence of the two frequency moments of the Li-Li spectra as $Q \to 0$ as well as the absolute values for the relaxation time. The former would imply that the "mode" will not be observable within the hydrodynamics realm, as the inequality condition given above is violated. Taken at its face value, this would confirm some predictions made from application of the revised Enskog theory [15], where the "fast sound" mode is expected to vanish at hydrodynamic scales. The persistence of a well defined peak down to 0.019 Å^{-1}, as will be shown below, seems to counter such an interpretation. As far as the relaxation time is concerned, notice that its extremely short values, which are more than one order of magnitude below those for the heavy component, imply that such a mode, even having a large velocity, cannot travel distances larger than very few atomic diameters, a result also found by experiment [11].

B. Approach to hydrodynamics

The extrapolated value for the hydrodynamic sound velocity of the alloy calculated from the hydrodynamic limit of

the static structure factor by recourse to Eq. (17) is of 2222 m/s. Such a figure is only 230 m/s above the experimental estimate from ultrasound techniques [5], which proves the adequacy of the potential here employed.

Some of the $R_{ij}(Q,\omega)$ partial structure factors for the region of the lowest accessible wave vectors are shown in Fig. 3. As seen there, both $R_{LiLi}(Q,\omega)$ and the $R_{LiPb}(Q,\omega)$ cross-correlation show rather sharp features in this range of wave vectors. Of particular relevance is the appearance of a strong Brillouin peak in the Li-Li correlation within the very same frequency where the Li-Pb function shows a strong, negative peak. The net result of this is a peak which is barely visible in the total structure factor for the lowest explored wave vector. The Brillouin frequency of the Li-Li peak at such a Q value is about 0.7 meV, which once converted into a phase velocity will yield a velocity of about 2874 m/s that is *substantially below* that of the "fast sound" mode inferred from spectra at larger wave vectors. In other words, the Li-Li partial structure factor shows that at low enough wave vectors the "fast sound" approaches the macroscopic sound velocity, in much the same way as found in a simulation for an He-Ne dense mixture [18].

The converse is also true for the spectrum of Pb-Pb correlations at the lowest wave vector. That is, the peak is now well resolved and shows a maximum frequency which corresponds to a velocity of about 2278 m/s, which is far above those measured at larger wave vectors for the Pb-Pb partial, even larger than the sound velocity in molten Pb, but approaches the hydrodynamic limiting value for the alloy.

An illustration of how the hydrodynamics is approached by the spectral frequency moments and by the Ω_Q frequencies is provided in Fig. 5. What seems worth emphasizing here is the approach to the linear dispersion regime given in terms of the sound velocity of the alloy by frequencies characterizing both partial spectra. The upper frame of Fig. 5 shows in full detail how the asymptotic limit for the ω_l moment corresponding to Li-Li correlations approaches a finite value of about 12 meV, as well as how departure from hydrodynamics occurs in a rather abrupt fashion above 0.1 Å^{-1} if Ω_Q frequencies are considered instead of ω_0. Such a distinct behavior is easily understandable by inspection of spectra shown in Fig. 4, where it is shown that such transition corresponds to the disappearance of the sharp features visible at low wave vectors.

A cursory glance to the upper frame of Fig. 5 would unveil the apparent contradiction between the calculated values of the reduced frequency moments for Li-Li and the presence of a peak at finite frequencies. In fact, from values for ω_0 and ω_l shown in that graph, it immediately comes out that the inequality Eq. (16) is being violated, and therefore a broad quasielastic response should be expected instead of the sharp features shown in Fig. 3. Such a discrepancy arises as a consequence of the complicated atomic dynamics within the alloy, which gives rise to spectra deviating from those expected for a single-component liquid. In fact, inspection of the graph for the Li-Li spectrum displayed in Fig. 3 for a wave vector of 0.260 Å^{-1} shows a line shape which is suggestive of the presence of more than one spectral component at a finite frequency. There is seen a maximum at about 4 meV concomitantly with an additional peak at about 13 meV, the lower frequency feature showing some analogies
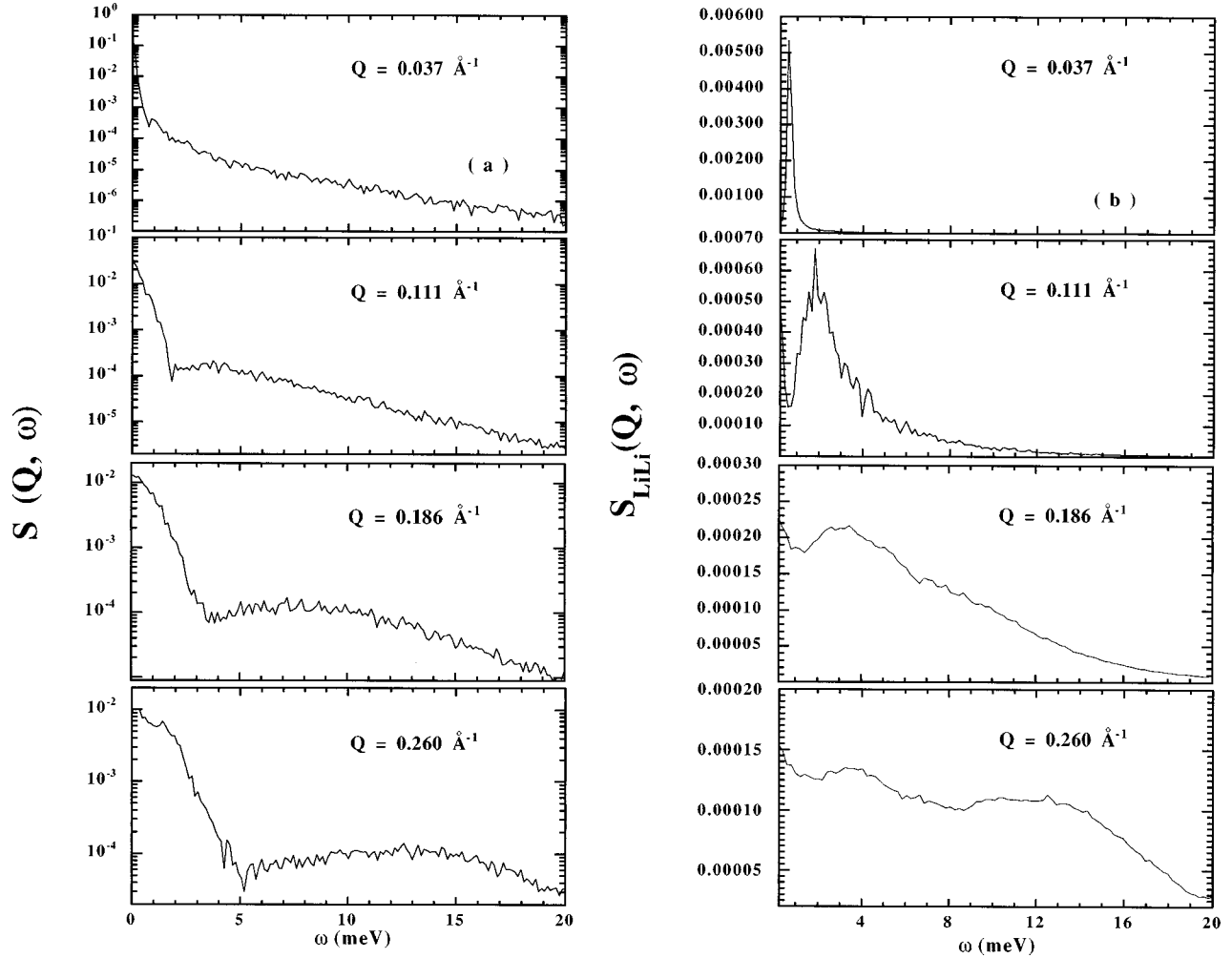
FIG. 3. Calculated partial structure factors for low wave vectors. The frames in (a) show the total $S(Q,\omega)$ for the alloy. It is shown on a semilogarithmic scale because of the strong quasielastic component. The different Q values are given as insets. (b)–(d) display the partial $S_{ij}(Q,\omega)$ spectra calculated for Li-Li, Li-Pb, and Pb-Pb correlations calculated for the same set of wave vectors. (e) displays spectra calculated for liquid Li. Units are meV^{-1}.

with that observed at 0.186 Å^{-1}. The line shape of the spectrum last referred to also deviates very substantially from that expected for a single-mode excitation in a liquid (i.e., a damped-harmonic oscillator [cf. Eq. (6) or a shape given by Eq. (13)]. In fact, although the spectrum shows only one maximum at finite frequencies, it appears to be superimposed on a broad decaying tail which reaches frequencies up to 30 meV. It is precisely the existence of such a broad signal which makes the ω_l moment to decrease with Q in a far smoother fashion than ω_0 (i.e., the higher frequencies contribute more strongly to ω_l than to ω_0), leading the former to a finite frequency intercept at $Q \rightarrow 0$. In opposition, the peak frequency, as measured without accounting for the large tail, is shown to be lower than ω_0, and approaches the macroscopic limit of the sound velocity of the alloy. More specifically, as Fig. 4 exemplifies, the contribution of the sharp peaks to the second moment amounts to about 20% of ω_0^2 for $Q = 0.037$ Å^{-1}, and a bare 15% at $Q = 0.186$ Å^{-1}.

In terms of frequencies of maxima of $J_l(Q,\omega)$, the Pb-Pb spectra show values for the phase velocity which decrease from that given above for 0.037 Å^{-1} to about 1166 m/s at $Q = 0.186$ Å^{-1}. Such a decrease in frequency of the "mode" corresponding to the heavy particle from the mac-

roscopic value is a well documented phenomenon. In fact, a strong drop in sound velocity from the adiabatic value as the wave vector is increased has been observed in a binary fluid mixture by Brillouin light scattering [20] for a dilute mixture of He into Kr. The phenomenon was understood semiquantitatively at that time [21] on the basis of linearized hydrodynamics and kinetic theory. It comes as a result of strong coupling between the acoustic and the concentration modes [22], which leads to a decrease in the sound frequency which is now given by a dispersion equation, which in the limit of small wave vectors reads [23]

$$\omega_B(x) = Qv_s \left[\pm i - \frac{1}{2} \frac{DQ}{v_s} \frac{v_s^2 - v_x^2}{v_x^2} \right], \quad (19)$$

where v_s stands for the adiabatic value of the sound velocity, and v_x represents the velocity of sound propagating at a constant value for the entropy derivatives $\delta S - (\delta S/\delta c)T, p \, \delta c$, where c represents the concentration. In other words, the coupling between the concentration and the acoustic mode makes the sound frequency steadily decrease as Q is increased, going from an adiabatic value at $Q = 0$ to v_x, which
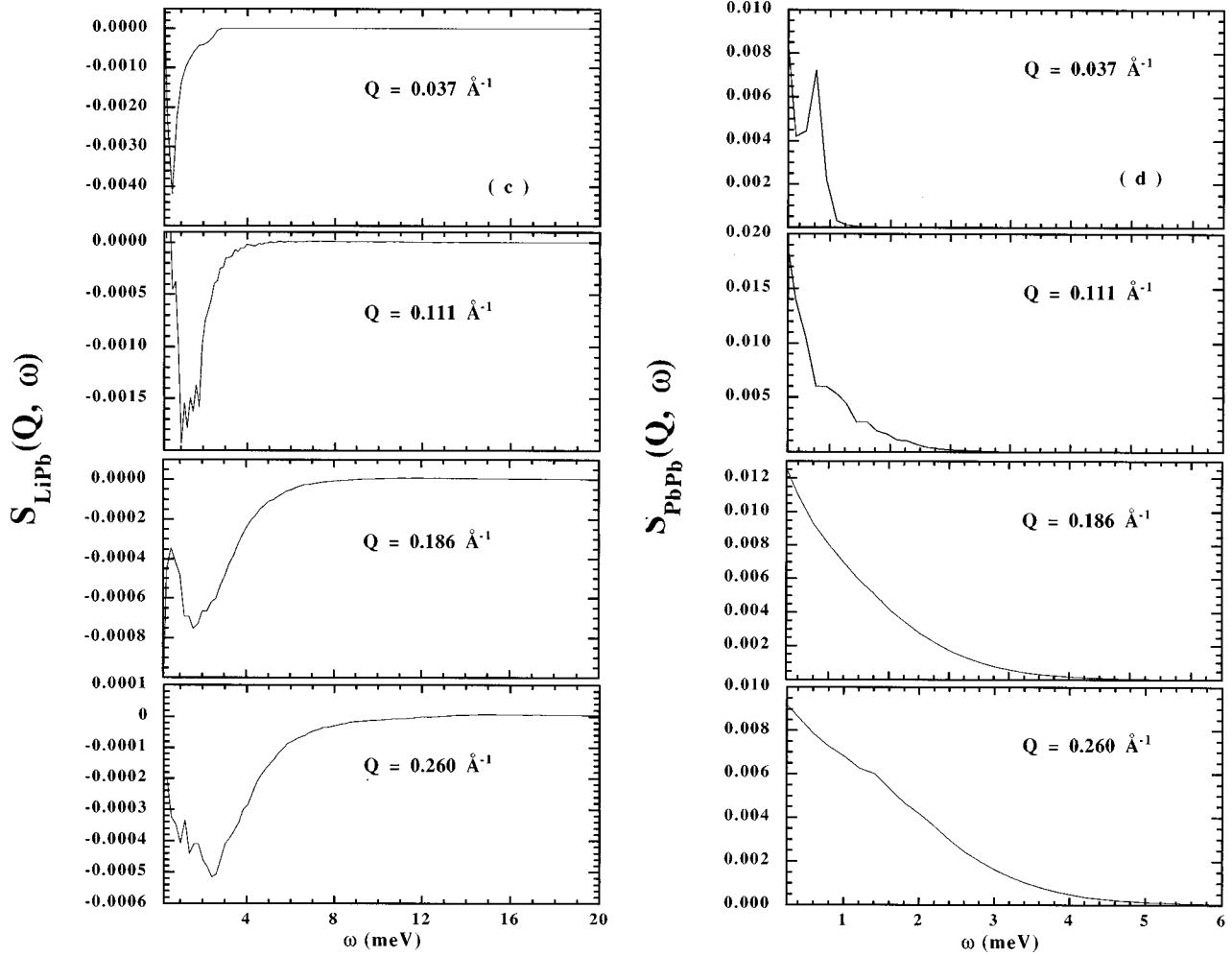
FIG. 3 (*Continued*).

is found to be substantially smaller [20]. Another important result from most of these treatments regards an additional term in the damping coefficient (the width of the Brillouin lines), which now contains, in addition to the frictional effects introduced by viscous and heat conduction, a term governed by the interdiffusion coefficient, so that the damping now becomes [21]

$$\Gamma_Q = \left(\frac{4\eta}{3\rho_m} + \frac{2}{3}D_T + \frac{5}{3}D + \frac{\rho_i \rho_j M_i M_j \rho}{3\rho M_{ij}} \right) Q^2, \quad (20)$$

where ρ_m is the average mass density, ρ_i is that for the ith species, D_T is the thermal diffusivity, η is the longitudinal viscosity, and $M_{ij} = M_i M_j / (M_j - M_i)$. Such an additional damping mechanism together with the reduced density account for the strong damping found for the Pb-Pb correlations, something which contrasts with the observation of well defined excitations up to large wave vectors in the pure liquid metal [13]. A comparison of spectra shown in Fig. 4 for liquid Li and the Li-Li partial also serves to illustrate the strong damping effect for the light component. As can be seen, the linewidth of the Brillouin peak in liquid Li is about one order of magnitude smaller at $Q = 0.260$ Å^{-1} than that of the Li-Li partial for the same wave vector. In other words, the additional term to sound damping dominates over viscosity and heat conduction effects.

The peak frequencies of both Pb-Pb and Li-Li partials show marked deviations below and above the hydrodynamic sound-frequency already at $Q = 0.111$ Å^{-1}. Also notice that the spectrum of Li-Pb correlations is mostly confined below 10 meV. In other words, for frequencies well beyond that limit, considering the Li dynamics as ''decoupled'' from that of the heavy particles as found in [8] seems fully justified.

C. Geometry of the atomic dynamics

A set of $D(r, \omega^\lambda)$ calculated for frequencies corresponding to characteristic zones of the ''dispersion curves'' shown in Fig. 2 are depicted in Fig. 6. A glance to such curves reveals that purely in-phase motions of *all* possible atom pairings, as shown by the positive peaks in $D(r, \omega^\lambda)$ appearing at the same positions than those in the static $g_{ij}(r)$ partial pair distributions, take place at low frequencies, and in fact, the phase coherence of these kinds of motions lasts up to about 6 meV. That is, a propagating sound wave involving all particles is sustained by the alloy up to rather high frequencies. The phase coherence of such motions is, however, limited for frequencies well below 20 meV, where, as seen from the graph, the Li-Pb atom pairs move purely out of phase (negative peak in the relevant correlation). An in-phase relationship up to relatively high frequencies persists for the Li-Li partial function, and some differences between
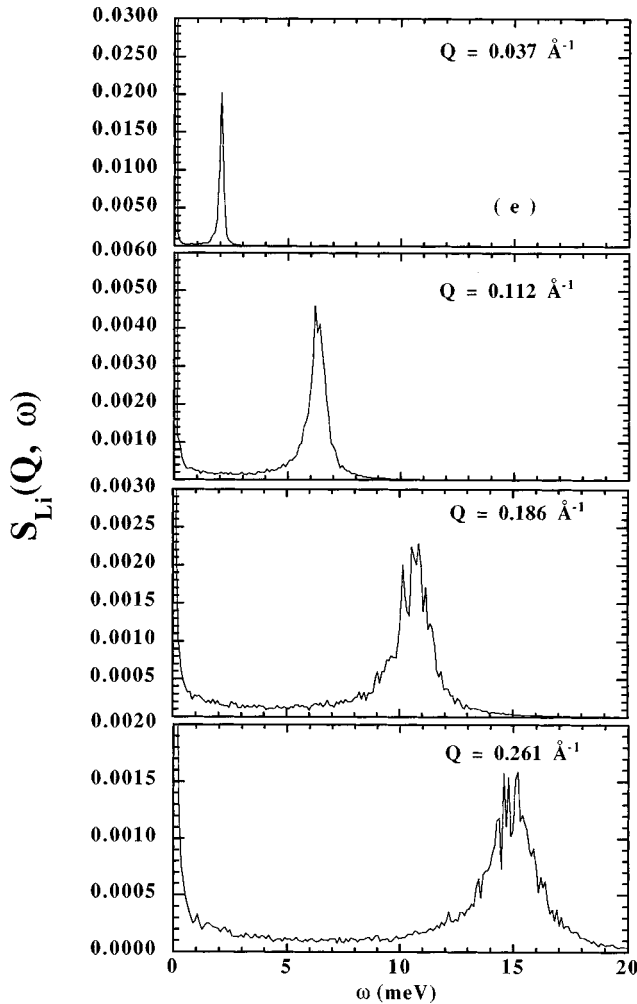
FIG. 3 (*Continued*).

that $D(r,\omega^\lambda)$ for Li within the alloy and the pure component are already seen at such frequencies. Such distinctive behaviors are amplified at larger frequencies. In particular, at frequencies of about 30 meV, the Li-Li pairs within the alloy show a curve which can be interpreted as either arising from motions characterized by antiparallel Cartesian-displacement vectors, or from motions executed by dynamically nonequivalent atoms. In contrast, the liquid metal exhibits close to purely out-of-phase motions at such frequency. As the maximum of the "dispersion curve" is approached (that is about 45 meV), all the $D(r,\omega^\lambda)$ functions show that the phase coherence with the respective $S_{ij}(Q)$ is definitely lost and the Li-Li pairs of the alloy exhibit a double-peak structure not found in the pure component.

As regards the spatial extent of the excitations, as inferred from the persistence of the oscillations $D(r,\omega^\lambda)$, it is found here that in accordance with theory [15] and previous simulation [8], the Li-Li correlations involve, at low frequencies, distances up to ≈ 8 Å, whereas both Li-Pb and Pb-Pb pairs show correlated motions involving the first coordination shells only. Notice, however, that such a relatively large "coherence length" is reduced with increasing frequencies, being confined to nearest neighbors for those corresponding to the top of the "dispersion curve."

D. Relationship with the dynamics of liquid Li

Our aim here is to compare some of the details of the dynamics of pure molten Li at temperatures just above melting (TS1), under conditions comparable to those of experiment [9], which evidenced a well defined collective mode, with those of Li within the alloy. To account for the temperature and density differences between liquid Li and the metal within the alloy, a series of simulations were also carried for a system composed of Li atoms at the same density as that of Li in Li_4Pb and the same temperature as the alloy (TS2).

The results of those calculations regarding the parameters defining the $R(Q,\omega)$ inelastic structure factors are shown in Fig. 7, the low-Q portion already shown in Fig. 5(c). Several noticeable differences between the parameters characterizing pure Li (irrespective of density and temperature) and Li within the alloy are readily seen from the graphs. The first concerns the rather different shape of the ω_0 and ω_l curves, especially regarding the low- and high-Q limits. Those for the pure metal approach both limiting behaviors in a way commensurate with that expected for a "simple liquid" as referred to in previous sections. The same applies to the relaxation time, and especially to the amplitude dependence of the peak integrated intensity with the wave vector, which now shows a well defined maximum at momentum transfers where the static structure factors show their maxima.

Particular attention is merited by the approach to hydrodynamics of the ω_0 curves, for both thermodynamic states. As seen in Fig. 7, the values taken at finite Q's approach the linear dispersion regime *from above*, that is, they exhibit a strong, positive dispersion. This causes the phase velocity to depart strongly from a hydrodynamic value of 4500 m/s and to reach 6580 m/s under conditions similar to those of the Li_4Pb sample. On the other hand, as shown in Fig. 5(c) the approach toward linear dispersion is followed by the ω_0 moment at wave vectors below 0.1 Å^{-1}.

As regards the lifetime of the excitations, a comparison of the relaxation times of both Li samples with those of the Li-Li partial of the alloy also shows a rather marked difference at low wave vectors. Those for Li metal show a very strong rise as one approaches the hydrodynamic limit, whereas those for the alloy are shown in Fig. 2 to follow a far smoother behavior, leading to an extrapolated value of the order of 0.1 ps.

In terms of the phase relationships of the atomic motions shown in Fig. 6(a), the most remarkable differences regard the somewhat more complex shape of the $D(r,\omega)$ curves for the pure metal at intermediate frequencies. A glance at the data of 20 meV shows that a pronounced negative peak is apparent at about 3.5 Å for molten Li, whereas the curve for Li within the alloy suggests that phase coherence is still retained.

As a final remark, let us focus on a comparison of the frequency spectra for Li within the alloy and that corresponding to liquid Li (TS1). Figure 8 depicts such a comparison in terms of the generalized frequency spectra for Li metal and for Li in the alloy. The most remarkable features show (a) the enhanced diffusion within the metal leading to a strong rise in $Z(\omega)$ at low frequencies, and (b) the appearance in both cases of a well defined shoulder at about 26
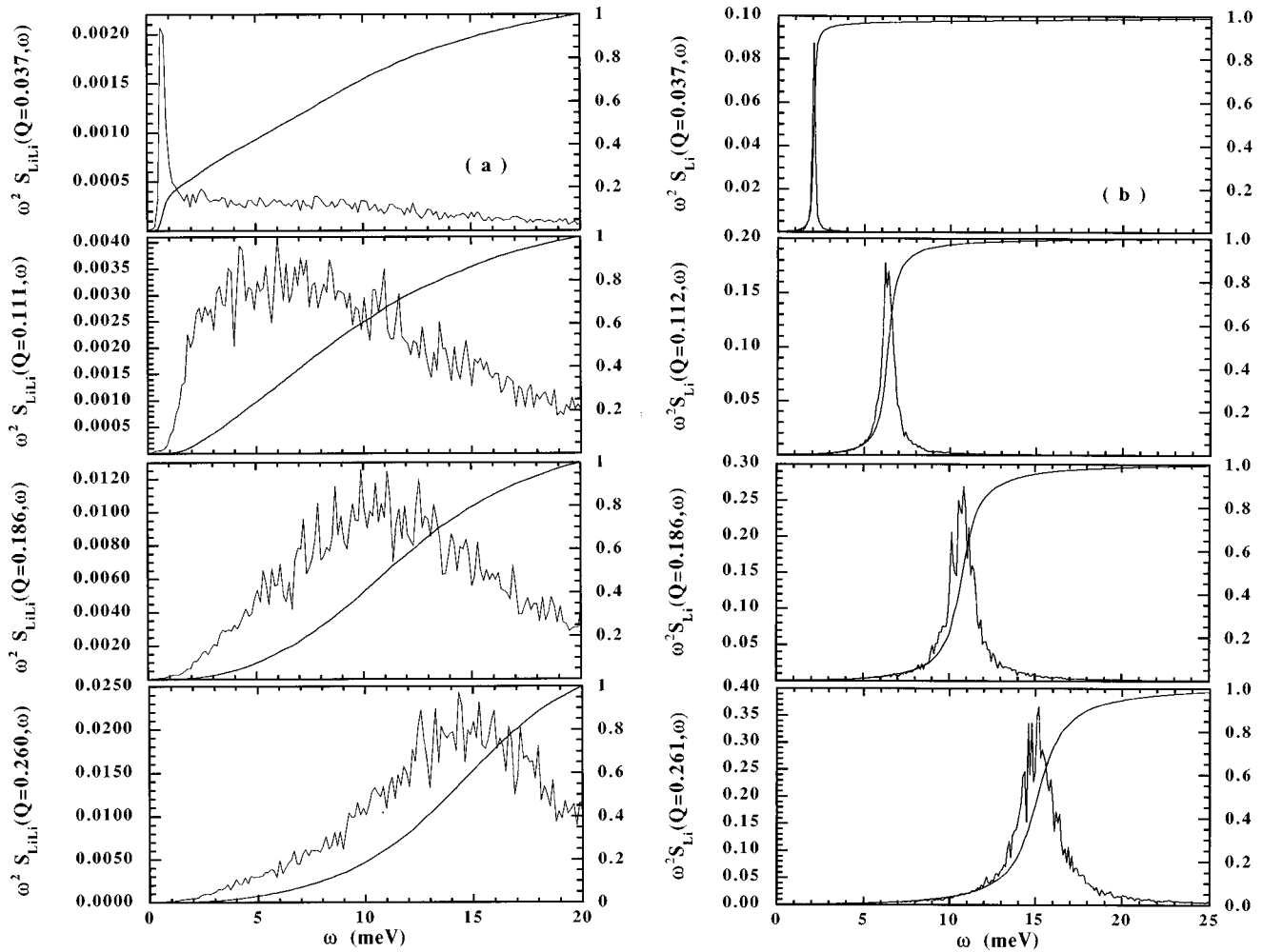
FIG. 4. Spectra of the longitudinal current-current correlation spectra at several wave numbers. (a) spectra for Li-Li correlations. The smooth curves show the percentage contribution to the second-moment integral up to a given frequency, and correspond to scales given on the right-hand side. (b) Same quantities for molten Li.

meV in the alloy and 32 meV in the pure metal. The spectrum then decays quite sharply for higher frequencies, in a way somewhat reminiscent of what has been found for liquid Ga [24], where such a high-frequency feature was shown to be correlated with higher-lying modes in some of its crystalline modifications. On the other hand, the presence of such a well defined shoulder can be related to the strong peak which appears at about 35 meV in the frequency distribution of cubic (bcc) Li at about 293 K [9]. In fact, data for the temperature dependence of the C_{11} elastic constant reported by Beg and Nielsen [9] show that, contrary to the transverse acoustic modes, the longitudinal excitation survives as a well defined entity up to temperatures as high as 0.94 times that of the melting point.

IV. DISCUSSION

A comparison between the frequencies derived from an analysis of the inelastic part of the experimental spectra and those calculated from fits to the simulated functions or as reduced frequency moments shows that computer simulations carried out with the specifications described above retain the most relevant details of the atomic high-frequency dynamics within the alloy. As known for quite some time

[21], only one propagating sound mode should appear within the realm of hydrodynamics, although nonhydrodynamic effects will be expected to have a profound effect on sound propagation. In fact, terms which are not present in the hydrodynamic description of monoatomic liquids, such as those describing the equilibration of momentum and temperature of the two species, are known to be characterized by rather low frequencies [21], and therefore will couple pressure and concentration fluctuations. Although the present results are limited by finite-size effects, it seems that both "sound velocities" for the light and heavy components will coalesce into a unique hydrodynamic mode at scales larger than a few hundred Å. This is best exemplified in terms of the phase velocities $v_{ph}^{i}(Q) = \Omega_Q/Q$ derived from maxima of the $J_l(Q,\omega)$ spectra, a result which is shown in Fig. 9. Notice from this that the departure becomes abrupt for both Li and Pb for wave vectors above 0.07 Å^{-1}, and that the phase velocities for Li match those calculated for the metal at larger momentum transfers.

If, as referred to in previous sections, the strong decrease in velocity for the heavy particle in a binary mixture is understood thermodynamically, the appearance of large deviations from hydrodynamic sound (positive dispersion) is
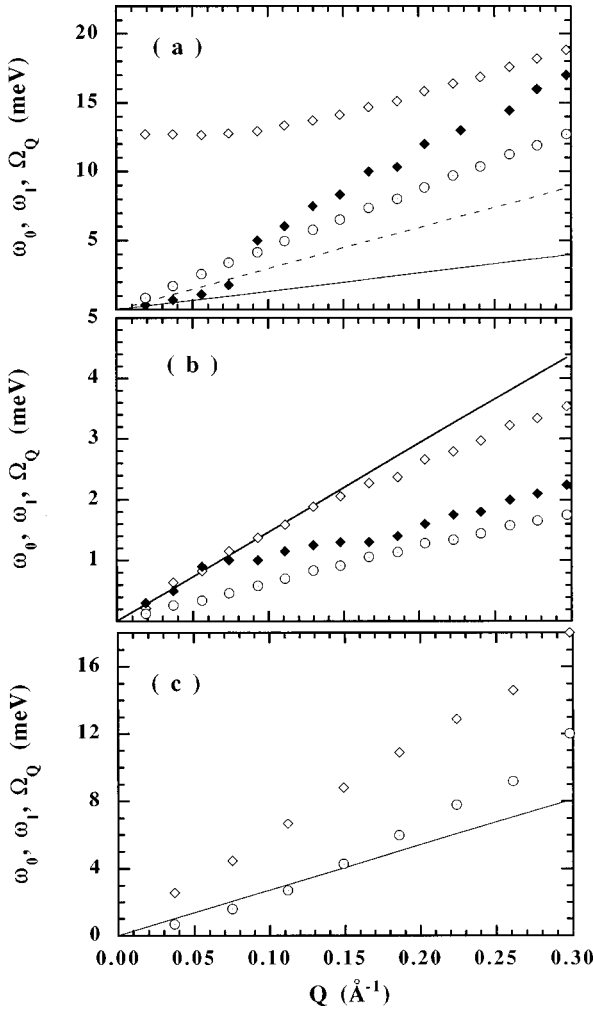
FIG. 5. Low-Q behavior of the reduced ω_0 (circles with a dot) and ω_l (lozenges) frequency moments as well as Ω_Q frequencies corresponding to peak maxima in $J_l(Q,\omega)$. The upper frame depicts such quantities for the Li-Li correlation within the alloy. The solid line shows the hydrodynamic dispersion of the alloy, and the dots depict the linear dispersion corresponding to pure molten Li. The middle frame shows the quantities characterizing the Pb-Pb correlations, and the lower frame corresponds to those for molten Li. The Ω_Q frequencies are not shown here because of their closeness to ω_0. The line depicts the linear dispersion for the molten metal.

known to be a characteristic of liquids composed by light particles such as liquid Li [25], and is probably a result of a variety of phonon interaction processes. Quantitative data on such deviations are available from experimental studies on other liquids, and have been shown to be large in those composed by light particles [26]. The deviation from hydrodynamics is conveniently described by [27]

$$\Delta\omega_Q = v_T \gamma Q^3 \frac{1 - Q^2/Q_a^2}{1 + Q^2/Q_b^2} \qquad (21)$$

where v_T is the hydrodynamic sound velocity, Q_b and Q_a are wave vectors corresponding to the maximum deviation from hydrodynamic sound and to the crossover to values of the phase velocity less than v_T, and γ controls the strength and kinematics of different interaction processes, whether instan-

taneous or through phonon-scattering mechanisms [27]. Fits to the data leaving v_T and Q_a fixed to the values of the hydrodynamic sound below and to the values corresponding to a crossover of ω_0/Q to velocities below sound (typically 1.1 Å^{-1} for liquid Li and about 1.5 Å^{-1} for Li$_4$Pb) yield estimates for γ of 78 (25) Å^2 and 287 (62) Å^2 (the difference between the latter two arising from the disparate values of the macroscopic sound velocity), which are much larger than those reported for any other liquid. This is easily understandable if, following Maris [27], one recalls that the probability of phonon-phonon interactions increases with increasing phonon energy. That is, for a classical sound wave, the scattering rate would be proportional to the energy of the wave, and therefore such a high-energy ''sound mode'' will provide very effective scattering channels. In other words, phonon absorption processes where the resultant phonon wave vectors are close to parallel (i.e., propagating in nearly the same direction) should be highly probable at such large energies. Such a picture is consistent with data regarding the excitations of other liquids such as superfluid ^{4}He at saturated vapor pressure (SVP) [28], where $v_T \approx 238$ m/s, and $\gamma = 1.11$ Å^{-1}, and deuterium [26], where $v_T \approx 1098$ m/s and $\gamma = 10.0$ Å^{-1}, as well as with the remarkably short lifetimes for the excitations found in both the pure Li metal and the alloy. The increase in the value for γ in going from liquid Li to Li$_4$Pb can then be rationalized in terms of the larger number of possible phonon interactions taking place in the alloy.

The analysis of the computer simulation data shows that both Li and Pb support collective ''modes'' with ''dispersions'' well above and below those corresponding to an extrapolation to long wave vectors of hydrodynamic sound. A description of the alloy in terms of two interpenetrating fluids seems adequate for momentum transfers above those corresponding to the maxima of the partial static structure factors. This is attested to by the approach of ω_0 to their ideal-gas limits [Eq. (11)], which shows that at such scales most collective effects in the dynamics have died away.

As shown above, the dynamics of liquid metallic Li, regardless of density and temperature differences with Li$_4$Pb, exhibits characteristics rather different from that of the same metal within the alloy. Although at moderately large wave vectors the dynamics of Li in metallic and alloyed states share a number of characteristics such as their frequencies and average polarizations, the different nature of both excitations becomes evident at both the low- and intermediate-Q ranges of spectra. As an illustration, it suffices to consider the very short lifetimes (i.e., the large width of the Li-Li spectra compared to those for molten Li). As shown in Figs. 2 and 7, the relaxation times for the Li-Li correlation in the alloy and that for the metal depart substantially as the wave vector is decreased, indicating that only the relaxation time for the metal goes to the expected hydrodynamic limit, (i.e., both lifetimes increase as $Q \to 0$, that for the metal showing a very fast increase below 0.1 Å^{-1}, whereas such an increase is far smoother for the alloy). Such a difference in the behavior with the wave vector of the relaxation times is reminiscent of that found for molecular liquids composed of heteronuclear dumbells [29], which, in fact, suggests that reorientations of Li$_4$Pb ''molecules'' may explain, in part, the differences in dynamics with the liquid metal.
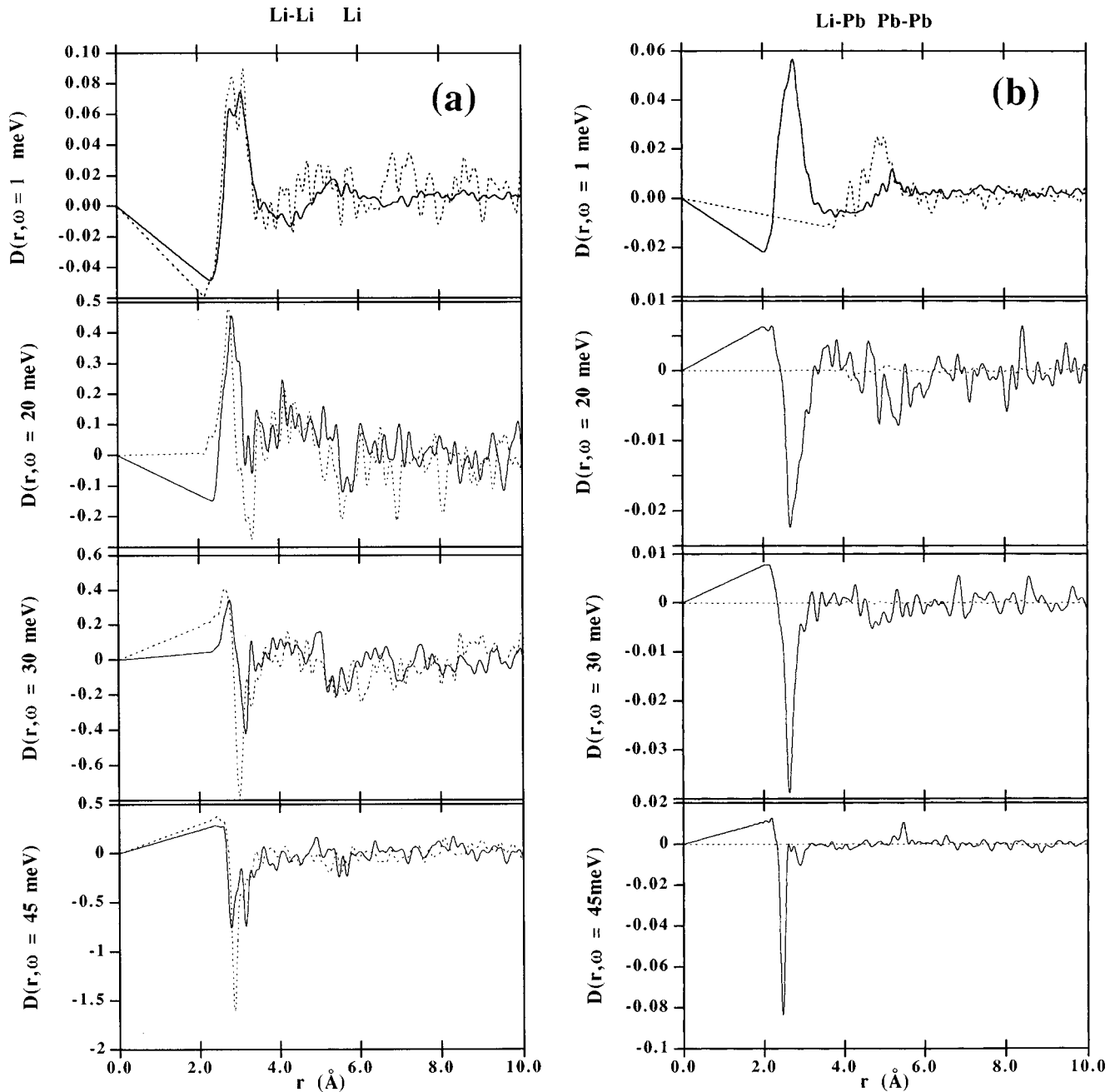
FIG. 6. $D(r,\omega)$ frequency dependent correlation functions (arbitrary units) corresponding to a set of normal-mode frequencies. Curves for Li-Li within the alloy are depicted as solid lines, whereas those for the pure molten metal are shown by dots. The Li-Pb cross-correlation is also shown by solid lines, whereas the Pb-Pb correlations are depicted by a dotted line. In the latter case the intensity of such correlations has been magnified five times.

At this point it seems worth delving into the analogies (and differences) between the characteristics of the observed excitation and those reported for molten salts. As established from experimental [12,30], computer simulation [31,32,8], and theoretical approximations [33], a well defined finite-frequency feature is expected to show up in the spectra of correlation functions for electrical charge or mass, or both. Whereas the appearance of a finite-frequency peak is common to all kinds of molten salts, irrespective of the mass difference between their constituent ions (in fact a well defined peak is present at the plasma frequency even in a one-component plasma), the persistence of a well defined

"mode" in the mass-mass correlations, not identifiable with an extension to large wave vectors of hydrodynamic sound, seems to be a characteristic of "asymmetric" salts, that is, those with a large mass difference between the two ionic species such are $Sr\,Cl_2$ simulated by De Leeuw [31] and measured by Margaca, McGreevy, and Mitchell [34], or RbCl and CsCl measured by McGreevy and co-workers [12,35] by cold neutron spectroscopy. In both cases, the spectra show a complex structure which arises from contributions to the intensity of more than one spectral component. The present results for Li_4Pb share with previous observations for RbCl and CsCl some analogies such is the presence
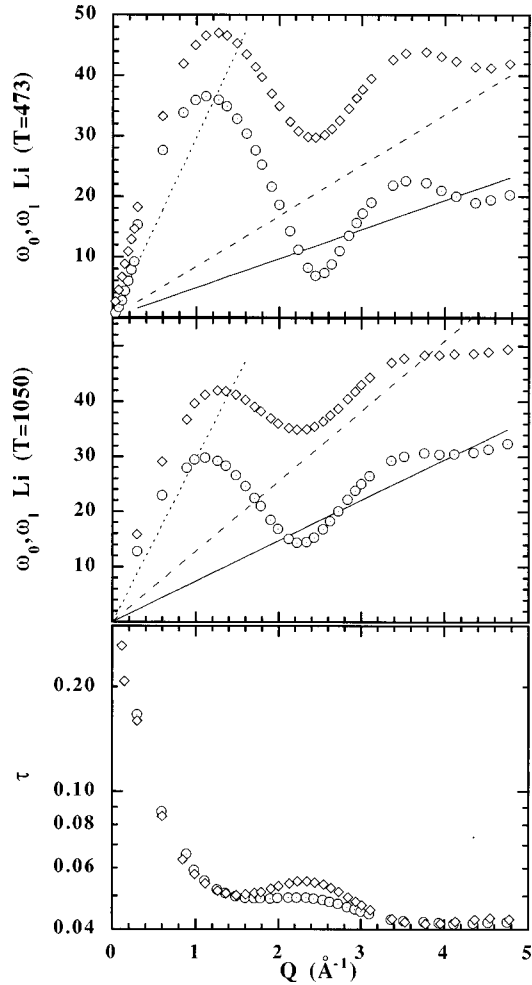
FIG. 7. Reduced frequency moments ω_0 and ω_l for liquid Li at the two thermodynamic states (see text). Units are in meV. Circles denote ω_0, lozenges stand for ω_l, and the solid and long-dashed lines give the ideal-gas limits. The dotted line shows the hydrodynamic dispersion. The lower frame depicts the relaxation times τ for Li at low (circles) and high (lozenges) temperatures.

of well defined peaks at high and low frequencies, although most of the reported experimental data result in fairly flat "dispersions" (possibly due to kinematic limitations). Such a behavior may arise from the partial ionic character of the
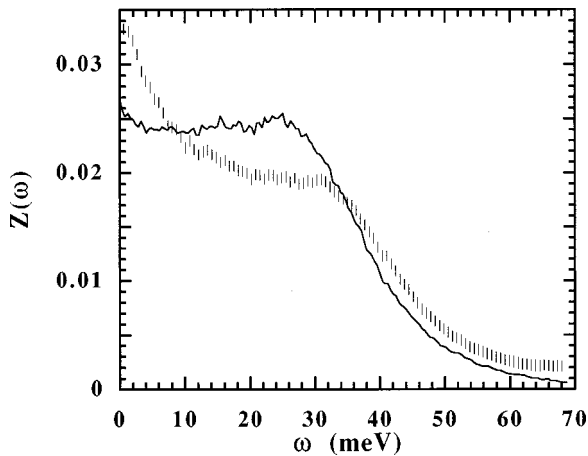

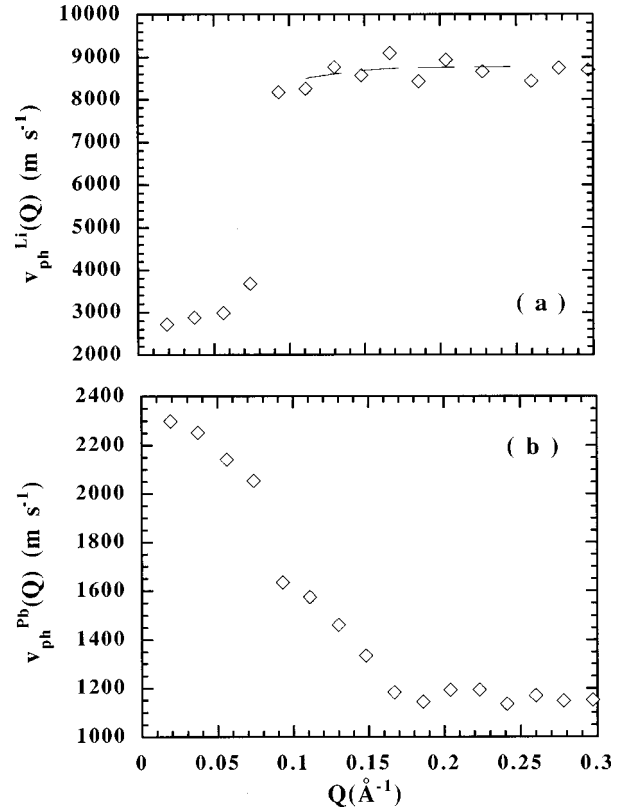FIG. 8. Frequency distributions of liquid Li (bars) and Li within the alloy (solid line). Units are meV^{-1}.

FIG. 9. Wave vector dependence of the phase velocities derived from the main maxima in $J_l(Q,\omega)$. The upper frame shows data for Li-Li (lozenges) compared to those for the molten metal (long dashes). The lower frame depicts data for Pb.

Li$_4$Pb alloy, an issue discussed many times in the literature [5].

V. CONCLUSION

The high-frequency "mode" in molten Li$_4$Pb, revealed by computer simulations [8], and later understood on kinetic theory [15] grounds, has recently been proved by experiment [11]. As predicted by theory and previous simulations, our results show that the peak seen at high frequencies arises from the dynamics of the Li atoms, shows a strong spatial dependence and, in agreement with experiment, its linewidth is characteristic of heavily damped excitations. The microscopic motions involved in such a high-frequency mode are significantly different from those involved in the propagation of a sound wave, as unequivocally demonstrated by comparison of the dynamics of liquid Li, under the same thermodynamic conditions as Li in Li$_4$Pb.

The departure of the high-frequency mode from hydrodynamic behavior is accompanied by the emergence of a "slow mode" involving the heavy particles only. The physical origin of the latter seems well understood on a hydrodynamic basis [21,22]. In opposition, the motions taking place at high frequencies are characterized by atomic motions with complex vector displacements, and approach purely out-of-phase displacements at frequencies close to the top of the "dispersion curve."

Finally, it is worth recalling that various theoretical conjectures [15] refer to the appearance of different propagation

frequencies which should merge with hydrodynamic sound dispersion at an appropriate length scale [15]. The present results confirm that sound propagation *sensu stricto* is confined to scales approaching the hydrodynamic realm, as attested to by the appearance of narrow peaks in the spectra for longitudinal current correlations.

Clear signatures of approaching a full hydrodynamic regime are found for the lowest explored wave vectors, which, in addition to a hydrodynamic mode corresponding to the in-phase motion of both kinds of particles of the alloy, show a broad nonhydrodynamic component in the Li-Li partial structure factor. Well within the microscopic regime the atoms move, showing more intricate phase relationships than those expected for an in-phase motion of the Li particles taking place against a matrix of stationary, heavy Pb atoms, with the possible exception of wave vectors close to $Q_{Li}/2$ where, as expected to occur in a crystal with two ions per primitive cell, the dynamics of the light and heavy particles can be considered as effectively decoupled.

[1] M. Rovere and M. P. Tosi, Rep. Prog. Phys. **49**, 1001 (1986).

[2] W. van der Lugt and W. Geertsma, J. Non-Cryst. Solids **61/62**, 187 (1984).

[3] J. A. Meijer, W. Geerstma, and W. van der Lugt, J. Phys. F **15**, 899 (1985).

[4] M. L. Saboungi, J. Marr, and M. Blander, J. Chem. Phys. **68**, 1375 (1978).

[5] H. Ruppersberg and H. Reiter, J. Phys. F **12**, 1311 (1982); A. P. Copestake, R. Evans, H. Rupersberg, and W. Schirmacher, *ibid.* **13**, 1993 (1983); J. H. Nixon and M. Silbert, Mol. Phys. **52**, 207 (1984).

[6] M. Soltwisch, D. Quitman, H. Ruppersberg, and J. B. Suck, Phys. Rev. B **28**, 5583 (1983); Phys Lett. **86A**, 241 (1981).

[7] S. W. Lovesey, *Theory of Neutron Scattering from Condensed Matter* (Oxford Science, Oxford, 1984), Vol. I, p. 221.

[8] J. Bosse, G. Jacucci, M. Ronchetti, and W. Schirmacher, Phys. Rev. Lett. **57**, 3277 (1986). See also G. Jacucci, M. Ronchetti, and W. Schirmacher, in *Condensed Matter Research Using Neutrons*, edited by S. W. Lovesey and R. Scherm (Plenum, New York, 1984), p. 139; G. Jacucci, M. Ronchetti, and W. Schirmacher, J. Phys. (Paris), Colloq. **8**, C-385 (1985).

[9] E. Burkel, *Inelastic Scattering of X-Rays With Very High Energy Resolution* (Springer, Berlin, 1991). For a comparison with the dispersion of crystalline ^{7}Li, see M. M. Beg and M. Nielsen, Phys. Rev. B **14**, 4266 (1976).

[10] P. H. K. de Jong, P. Verkerk, C. F. de Vroege, L. A. de Grraf, W. S. Howells, and S. M. Bennington, J. Phys.: Condens. Matter **6**, L681 (1994).

[11] M. Alvarez, F. J. Bermejo, P. Verkerk, and B. Roessli, Phys. Rev. Lett. **80**, 2141 (1998).

[12] See, for instance, R. L. McGreevy, E. W. J. Mitchell, and F. M. A. Margaca, J. Phys. C **17**, 775 (1984).

[13] O. Söderstrom, J. R. D. Copley, J. B. Suck, and B. Dorner, J. Phys. F **10**, L151 (1980).

[14] Some useful remarks about the meaning of fit parameters arising from the use of the DHO function are given in H. R. Glyde, *Excitations in Liquid and Solid Helium* (Clarendon, Oxford, 1994), pp. 184 and 185.

[15] A. Campa and E. G. D. Cohen, Phys. Rev. Lett. **61**, 853 (1988); Phys. Rev. A **41**, 5451 (1990); P. B. Lerner and I. M. Sokolov, Physica C **150**, 465 (1988).

[16] R. Fernández-Perea, F. J. Bermejo, and E. Enciso, Phys. Rev. B **53**, 6215 (1996).

[17] N. H. March and M. P. Tosi, *Atomic Dynamics in Liquids* (Macmillan, New York, 1977).

[18] E. Enciso, N. G. Almarza, P. Domínguez, and F. J. Bermejo, Phys. Rev. Lett. **74**, 4233 (1995).

[19] The procedure was developed by J. M. Carpenter and C. A. Pelizzari, Phys. Rev. B **12**, 2397 (1975), and applied several times to the analysis of neutron scattering data from amorphous materials. See, for instance, A. C. Hannon, M. Arai, and R. G. Delaplane, Nucl. Instrum. Methods Phys. Res. A **354**, 96 (1995).

[20] B. Y. Baharudin, P. E. Schoen, and D. A. Jackson, Phys. Lett. **42A**, 77 (1972).

[21] N. A. Clark, Phys. Rev. A. **12**, 2092 (1975). See also R. D. Mountain and J. M. Deutch, J. Chem. Phys. **50**, 1103 (1969).

[22] J. P. Boon and S. Yip, *Molecular Hydrodynamics* (McGraw-Hill, New York, 1980), p. 269.

[23] H. N. W. Lekkerkerker and J. P. Boon, Phys. Lett. **39A**, 9 (1972).

[24] F. J. Bermejo, R. Fernández-Perea, M. Alvarez, B. Roessli, H. E. Fischer, and J. Bossy, Phys. Rev. E **56**, 3358 (1997).

[25] A. Torcini, U. Balucani, P. H. K. de Jong, and P. Verkerk, Phys. Rev. E **51**, 3126 (1995).

[26] M. Mukherjee, F. J. Bermejo, B. Fåk, and S. M. Bennington, Europhys. Lett. **40**, 153 (1997).

[27] H. J. Maris, Rev. Mod. Phys. **49**, 341 (1977).

[28] *Excitations in Liquid and Solid Helium* (Ref. [14]), p. 187.

[29] S. H. Chong and F. Hirata, Phys. Rev. E **57**, 1691 (1998).

[30] J. R. D. Copley and A. Rahman, Phys. Rev. A **A13**, 2276 (1976).

[31] S. W. de Leeuw, Mol. Phys. **37**, 489 (1979).

[32] E. M. Adams, I. R. McDonald, and K. Singer, Proc. R. Soc. London, Ser. A **357**, 37 (1977).

[33] J. P. Hansen, in *Amorphous Solids and the Liquid State*, edited by N. H. March, R. A. Street, and M. Tosi (Plenum, New York, 1985), p. 229.

[34] F. M. A. Margaca, R. L. McGreevy, and E. W. J. Mitchell, J. Phys. C **17**, 4725 (1984).

[35] R. L. McGreevy, E. W. J. Mitchell, F. M. A. Margaca, and M. A. Howe, J. Phys. C **18**, 5235 (1985).